Available online at www.sciencedirect.com
SCIENCE DIRECT®
Catalysis Today 89 (2004) 89–95
CATALYSIS TODAY
www.elsevier.com/locate/cattod

Synergistic effect of silent discharge plasma and catalysts on benzene decomposition

Shigeru Futamura [a,*], Hisahiro Einaga [a], Hajime Kabashima [a], Lee Yong Hwan [b]

[a] National Institute of Advanced Industrial Science and Technology, AIST Tsukuba West, 16-1 Onogawa, Tsukuba, Ibaraki 305-8569, Japan
[b] School of Environmental Science and Engineering, Pohang University of Science and Technology, San-31, Hyoja-dong, Nam-gu, Pohang, Kyungbuk 790-784, Republic of Korea

Abstract

Methods for hybridization of silent discharge plasma and catalysts in different forms are presented, and their synergy in benzene decomposition is discussed. TiO_2 deposition on the inside wall of the coaxial type of the silent discharge plasma reactor promotes benzene decomposition in air and increases CO_2 yield. TiO_2–silica gel granules housed inside of the punched internal electrodes also facilitate the oxidative decomposition of benzene. Comparison of the TiO_2 surface before and after the reactions by FTIR suggests that the positive effect of TiO_2 can be ascribed to the active oxygen species generated on its surface. Replacement of TiO_2–silica gel by MnO_2 also promotes the oxidative decomposition of benzene in silent discharge plasma. Ozone, which is generated from gaseous oxygen, is decomposed by MnO_2, but not by TiO_2. Catalytic effects of TiO_2 and MnO_2 can be ascribed to formation of active oxygen species on their surfaces and that of the triplet oxygen atom from ozone on the MnO_2 surface. It has been shown that both of TiO_2 and MnO_2 can sustain their catalytic activities in silent discharge plasma.

Keywords: Benzene; Decomposition; Silent discharge plasma; Photocatalysts; Catalysts; Synergy

1. Introduction

Nonthermal plasma has attracted much attention as an energy-saving method for VOCs control for this decade [1–16] due to its unique properties such as quick response at ambient temperature, achievement of high electron energies within short residence times, system compactness, and easy operations. This technique is especially effective in removing olefinic VOCs such as trichloroethylene, tetrachloroethylene, and ethylene at smaller energy consumptions [6]. Emission of volatile aromatic hydrocarbons is also of great social concern due to their carcinogenicities and respiratory disorders. This compound class is one of the viable targets, but their reactivities in nonthermal plasma are not satisfactorily high. It is desperately required to develop an energy-efficient method based on nonthermal plasma.

One of the options is use of catalysts for the oxidative decomposition of aromatic hydrocarbons. Ozone, which is abundantly formed from O_2 in silent discharge plasma reactors [13], can be utilized as the oxidant precursor in the catalyst bed set on the downstream of the silent discharge plasma reactor. It has been shown that manganese oxide catalysts simultaneously promote the ozone decomposition and benzene oxidation [14,15].

Another possibility is activation of catalysts or photocatalysts hybridized in nonthermal plasma reactors. It is already known that the ordinary photocatalyst TiO_2 can be activated by emission lights from the excited states of nitrogen molecules in the silent discharge plasma reactor [17]. If the light intensity is strong enough to activate photocatalysts neatly incorporated inside of the reactor, active oxidants such as OH radicals, O^-, and O_3^- can be generated from O_2. Under these conditions, the synergy between nonthermal plasma and TiO_2 is anticipated in promoting benzene decomposition since it is an effective photocatalyst in this reaction [18,19].

In this research, a coaxial type of silent discharge plasma reactor has been chosen to hybridize nonthermal plasma with catalysts in different forms in different ways. This paper describes the experimental methods for hybridization of nonthermal plasma and catalysts and discusses their synergy in benzene decomposition.

* Corresponding author. Tel.: +81-29-861-8497; fax: +81-29-861-8266.
E-mail address: s-futamura@aist.go.jp (S. Futamura).

0920-5861/$ – see front matter © 2003 Elsevier B.V. All rights reserved.
doi:10.1016/j.cattod.2003.11.014

2. Experimental

2.1. Catalyst materials

MnO_2 pellets were purchased from Kanto Kagaku, Co., Ltd. They were pulverized and the granules of diameter in 1.18–1.70 mm were collected for use. TiO_2 P25 (surface area: 43 $m^2\,g^{-1}$) was used without further purification.

TiO_2–silica gel pellets HQA 12 (particle size: ~1.7 mm, TiO_2 loading rate: ~13%, surface area: 300 $m^2\,g^{-1}$, average pore diameter: 10 nm, pore volume: 0.8 $ml\,g^{-1}$) were purchased from Sinto V Cerax, Co., Ltd., and used as received.

2.2. Characteristics of a plasma reactor

A silent discharge plasma reactor (SDR) used in this research was a tubular type consisting of a stainless steel rod coated with different kinds of metals such as copper (Cu), aluminum (Al), and stainless steel (SUS316) (o.d. 8.6 mm) and an encircling glass tube (i.d. 10.6 mm), which was wrapped with aluminum foil (100 mm wide) (Fig. 1a) [13]. This original model was used to hybridize TiO_2 powders on the inside wall of the outer glass vessel of SDR (Fig. 1b). Instead of the metal jacket, punched electrodes of SUS316 (punch) were prepared and used to house TiO_2–silica gel pellets (Fig. 1c). The diameters of pinholes were 1 mm and their density was 25 cm^{-2}. Table 1 summarizes the combinations of reactor geometry and catalyst. SDR was energized with 50 Hz sine wave ac up to 8–11 kV rms. The gas residence time varied in the range of 0.36–1.80 s at 0.5–0.1 l/min of gas flow rate.

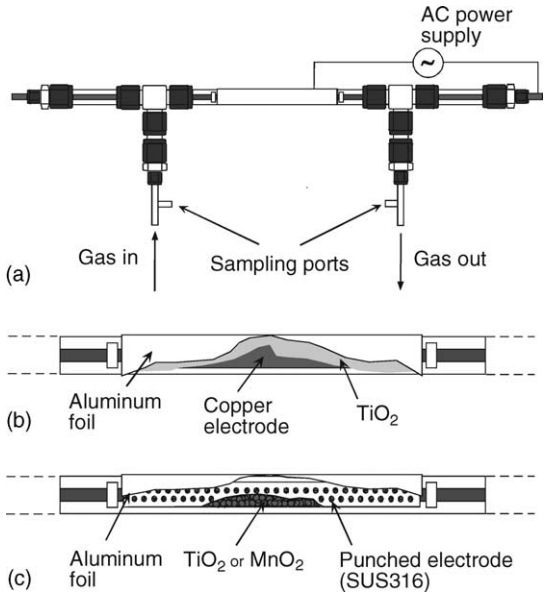

Fig. 1. Methods for hybridization of SDR with catalysts or photocatalysts. (a) SDR, (b) SDR whose inside wall of the outer glass tube is coated with TiO_2, (c) SDR whose internal punched electrode houses catalyst/photocatalyst pellets.

Table 1
Combinations of reactor geometry and catalyst

Reactor-catalyst	Reactor geometry in Fig. 1
SDR-none	(a)
SDR-TiO_2	(b)
SDR-MnO_2	(c)
SDR-HQA 12	(c)

2.3. Hybridization of SDR and catalysts

Method 1. Aqueous suspensions of TiO_2 were coated on the ground surface of the inside wall of the glass tube, which was dried at 373 K for 1 h. The amount of TiO_2 deposited was ca. 60–70 mg.

Method 2. Catalyst or photocatalyst pellets such as MnO_2 (6.06 g) and HQA 12 (1.9 g) were packed inside of punch and dried in a oven at 393 K for 19 h before use. After the electrode temperature was cooled down to room temperature, it was fabricated into SDR.

2.4. Plasma chemical decomposition of benzene

Benzene balanced with N_2 in a standard gas cylinder was introduced to the reactor through a Teflon tube after its dilution by N_2 and O_2 in separate gas cylinders. The gas flow rate and the concentrations of benzene and O_2 were adjusted with sets of mass flow controllers and a gas mixer.

After each run, air was passed through SDR at 7 kV for 20 s to oxidatively remove the carbonaceous materials deposited on the catalysts and the inside wall of SDR.

2.5. Photochemical decomposition of benzene

The photochemical reactor was fabricated from Pyrex glass with a quartz glass window, and contained a square shaped glass plate (50 mm × 45 mm). The catalyst was coated on one side of the glass plate.

Photoirradiation was carried out for the catalyst through the quartz glass window by a 500 W high pressure Hg lamp equipped with a band path filter (365 nm). The numbers of photons were counted by potassium ferrioxalate actinometry according to the literature method [20].

2.6. Analysis

The values of plug-in power and applied voltage for SDR were measured with a digital powermeter (YOKOGAWA WT 110) and a digital wavemeter (SONY TEKTRONIX STA 55 W), respectively. Combination of a model of high voltage amplifier 20/20B (Trek Japan, Co., Ltd.), a function generator (FG-2, Wavetek), and an oscilloscope (SONY TEKTRONIX TDS 3052) was used instead of a Neon transformer to estimate the power consumptions in SDR. Fig. 2 shows the typical voltage and current waveforms in SDR. The reactor power consumptions were calculated from the

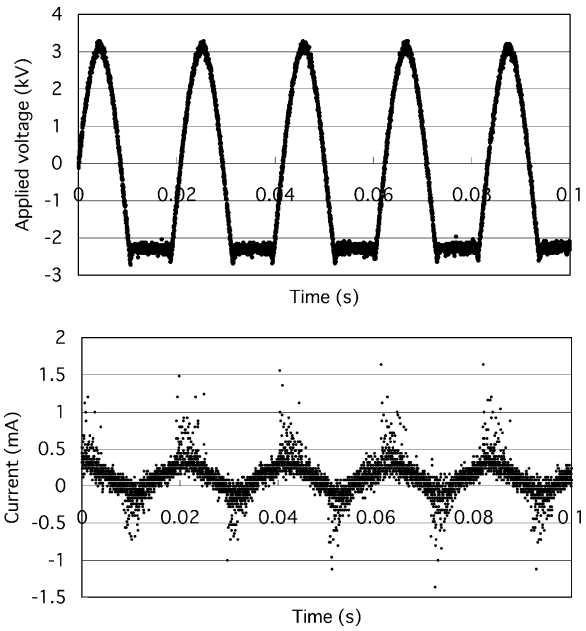

Fig. 2. Typical waveforms of voltage and current in SDR. Gas composition N_2:O_2 = 4:1 (v/v), gas flow rate 500 ml/min, 50 Hz sine wave ac from 20/20B.

integration of the power waveforms [13]. In the applied voltage range of 3–11 kV, data sets of power consumptions in SDR, applied voltages, and benzene conversions were obtained with 20/20B as the power supply. Then, the data sets to relate reactor power consumption to benzene conversion were collected at different levels of applied voltage with the Neon transformer. Based on the comparison of these data, it was shown that about 20 ± 3% of plug-in power was consumed in SDR for benzene decomposition with the Neon transformer as the power supply. The volatile byproducts were identified by GC-MS [Shimadzu QP-5050A (EI, 70 eV)-GC-17A]. The benzene conversions and byproduct yields were determined by GC [GC 353 (GL Sciences)]. The O_3 concentrations were measured on a UV photometric analyzer, SOZ-6300 (Seki Electronics). Product identification and quantification of benzene, ozone, CO, and CO_2 were also carried out by FTIR (JASCO FT/IR 480 Plus equipped with a 2.4 m gas cell and a triglycine sulfate (TGS) detector). Diffuse FTIR spectra of the TiO_2 samples before and after reactions were taken in a diffuse reflectance cell (JASCO DR-81) with KBr as a standard (resolution: 4 cm^{-1}). The collected data were processed with Kubelka-Munk Transform.

As a measure of the energy efficiency for SDR, reactor energy density (RED) is used later (Eq. (1)). The conversion factor of 0.2 denotes the ratio of reactor power to plug-in power for SDR based on the measurements of power consumptions described above

$$\text{RED (kJ/l)} = 0.2 \times \frac{\text{plug-in power (kW)}}{\text{flow rate (l/s)}} \quad (1)$$

3. Results and discussion

3.1. Synergy between SDR and MnO_2

According to our previous data with SDR, no correlation was observed between the amount of O_3 formed from gaseous oxygen and the conversions of VOCs such as trichloroethylene (TCE) [13], benzene [14], and CH_3Br [12] under aerated conditions. Interestingly, only the decomposition of TCE was promoted by gaseous oxygen without catalysts. Our hypothesis was that the triplet oxygen atom [$O(^3P)$], which was formed directly from the dissociation of O_2 and indirectly from the ozone decomposition, promoted the oxidative decomposition of TCE. The kinetic data support that $O(^3P)$ is more reactive with TCE than with benzene [21,22]. These experimental and reference data urged us to generate $O(^3P)$ in higher concentrations in reaction gases. It has been already reported that the serial combination of the MnO_2 pellet bed to the outlet of SDR is effective in simultaneously decomposing ozone and benzene [14]. Before catalysts were hybridized with SDR, effect of the internal electrode material was investigated. No change was observed for the relationship between plug-in power and applied voltage by replacing Cu electrode by Al, SUS, and punch (Fig. 3). Next, ozone concentrations were measured with these electrodes since the efficiency of ozone formation could be used as a parameter reflecting plasma strength in SDR. Fig. 4 shows that almost the same levels of ozone were obtained, irrespective of electrode materials and forms as long as the gap distance is fixed. All these data clearly show that the same plasma properties are obtained even with punch.

Fig. 5 shows the catalytic effect of MnO_2 in benzene decomposition in O_2. The conversion data were collected 3 h after the onset of gas flow to assure the achievement of the adsorption–desorption equilibrium for benzene on MnO_2. Since the increments of benzene conversion at fixed REDs increased with RED, the time profile of the benzene conversion was depicted in the absence and presence of MnO_2

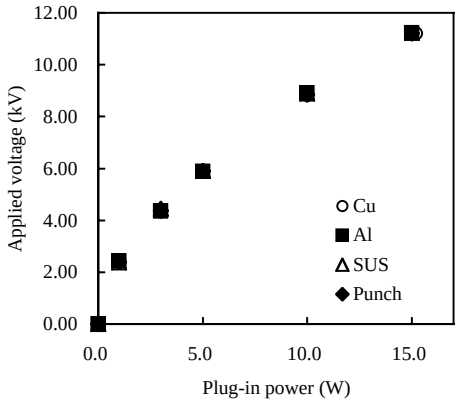

Fig. 3. Effect of internal electrode metals in SDR on the relationship between plug-in power and applied voltage. Gap distance: 0.7 mm, gas: O_2, Q = 500 ml/min.

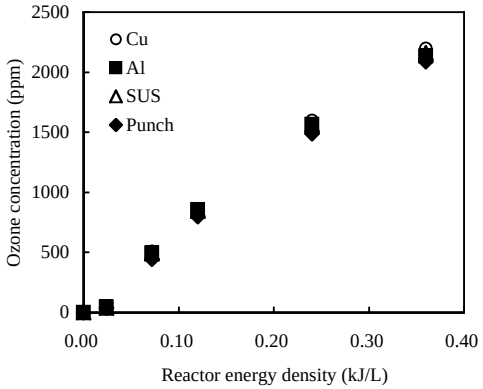

Fig. 4. Effect of internal electrode metals in SDR on ozone formation. Gap distance: 0.7 mm, gas: O_2, $Q = 500$ ml/min.

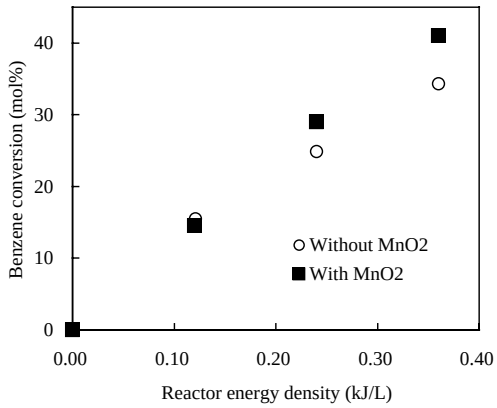

Fig. 5. Additive effect of MnO_2 on benzene conversion in air. Gap distance: 1.0 mm, benzene: 105 ppm, $Q = 500$ ml/min.

at 0.36 kJ/l of RED (Fig. 6). In the absence of MnO_2, the benzene conversion was almost constant at 34%, but it increased with time in the presence of MnO_2. The 20 min after the data collection was started, benzene conversion tended to level off at ca. 54%. As Fig. 7 shows, MnO_2 decomposes O_3 generated in SDR. These findings suggest that the oxygen atoms are formed on the surface of MnO_2 (O^*) and a part of desorbed O^* is present as $O(^3P)$ in the gaseous phase (Fig. 8). These oxygen atoms are possible oxidants in this reaction. $MnO_2(OH)_4$ can be another candidate for benzene oxidation [23,24], but this species is less likely to

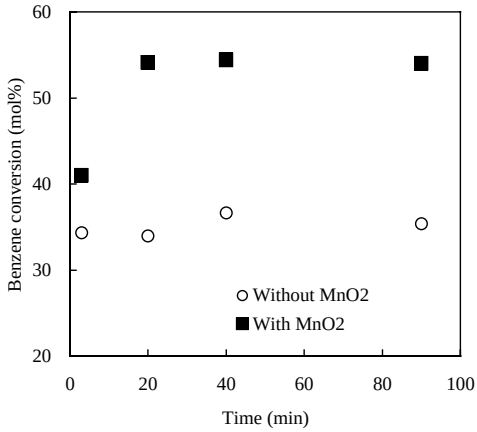

Fig. 6. Time profile for the additive effect of MnO_2 on benzene conversion in air. Gap distance: 1.0 mm, benzene: 105 ppm, $Q = 500$ ml/min, RED = 0.36 kJ/l.

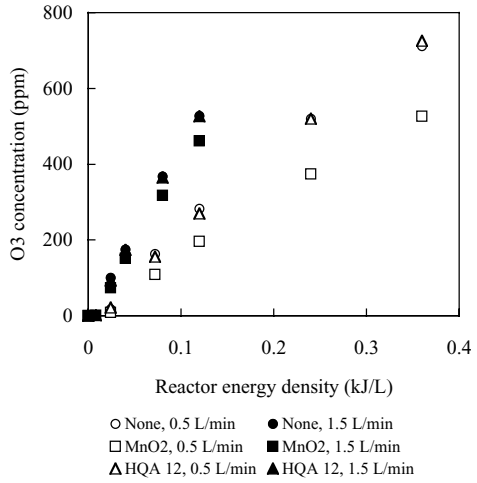

Fig. 7. Effect of MnO_2 and HQA 12 on ozone decomposition in O_2.

be involved because it is formed from $O_2{}^*$, which is formed in the secondary Rideal-Eley Type Reaction of O^* and O_3 (Fig. 8).

No change was observed in the activities of fresh and the used MnO_2 samples for ozone formation from O_2 in the gas flow rate range of 0.5–1.5 l/min (Fig. 9). Deactivation of MnO_2 is neglected in our experiments.

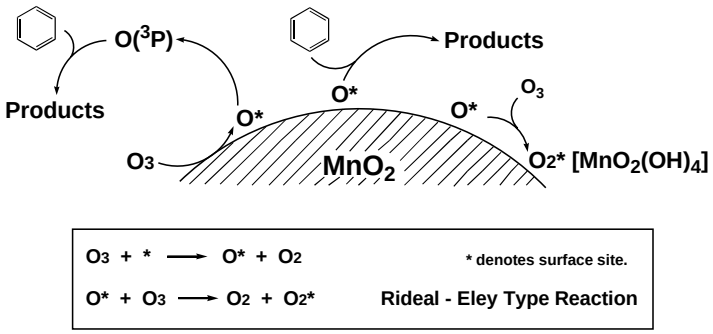

Fig. 8. Mechanism for MnO_2-catalyzed oxidation of benzene.

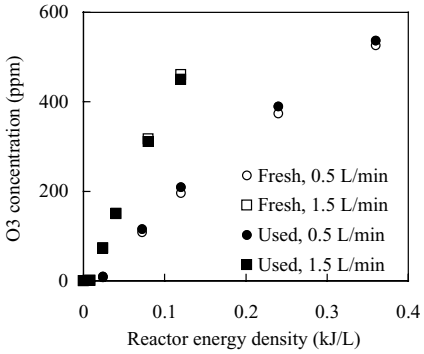

Fig. 9. Catalytic effect of the fresh and used MnO_2 on O_3 decomposition in O_2.

3.2. Synergy between SDR and TiO_2

Fig. 10 shows the synergistic effect of SDR and TiO_2 coated inside wall of the outer glass tube of SDR in benzene decomposition in dry air. The reaction was started by energizing SDR after the adsorption–desorption equilibrium of benzene on TiO_2 was achieved (∼3 h). Benzene conversion and the concentrations of CO and CO_2 were obtained in the steady state. With an increase in RED, benzene conversion (Fig. 10a) and the amounts of CO and CO_2 (Fig. 10b) monotonously increased. At 0.84 kJ/l of RED, benzene conversion doubled and CO_2 amount increased on TiO_2 addition, while CO amount did not change apparently. These findings suggest that the synergy between SDR and TiO_2 can be expected at residence times shorter than 2.0 s. Carbon balance in this reaction (ratio of the amount of CO_x formed to that of the benzene consumed) was improved with an increase in RED, but it fell in 30–70% with TiO_2 although it varied in 75–95% without TiO_2. Relatively low carbon balances in the presence of TiO_2 are ascribed to carbon deposits on the TiO_2 surface. Deposition of Rh on TiO_2 is effective in improving the TiO_2 durability by inhibiting the formation of carbon deposits on the catalyst surface and accelerating their decomposition [25].

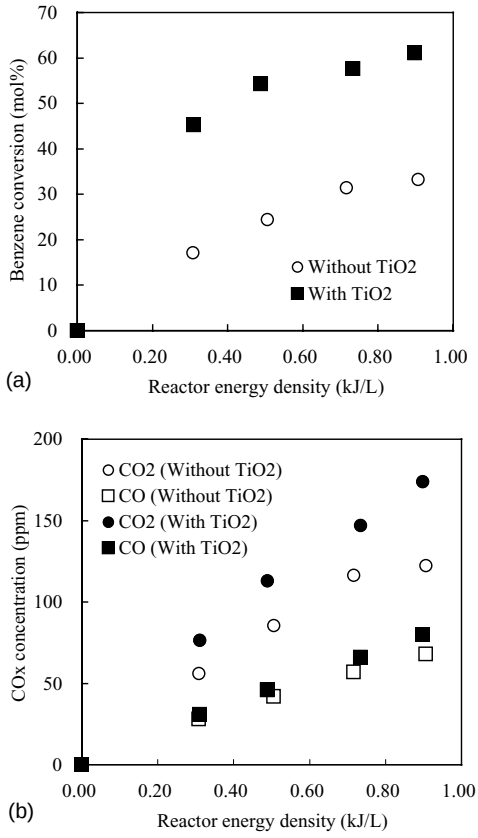

Fig. 10. Effect of TiO_2 coating on benzene decomposition in air. Gap distance: 1.0 mm, benzene: 100 ppm, $Q = 100$ ml/min. (a) Benzene conversion, (b) concentrations of CO and CO_2.

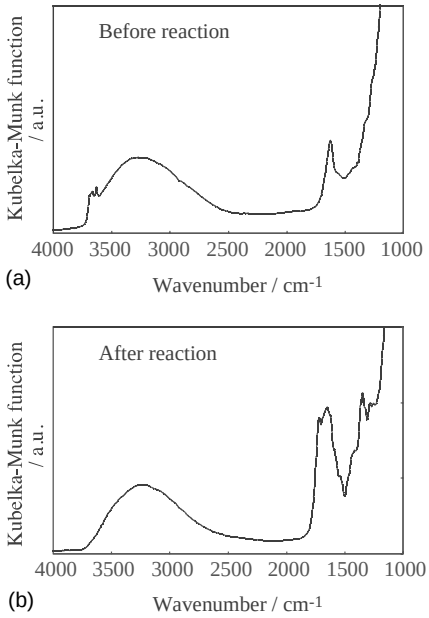

Fig. 11. Diffuse reflectance FTIR spectra of TiO_2 on the inside wall of the outer glass tube of SDR. (a) Before reaction, (b) after reaction.

After reactions, the color of TiO_2 turned yellow from white. Fig. 11 comparatively shows the diffuse FTIR spectra of the TiO_2 samples before and after the reaction. Before the reaction (Fig. 11a), absorption bands of water physically adsorbed on TiO_2 are observed at 1620 and 2600–3650 cm^{-1} and those of surface hydroxyl groups at 3650–3700 cm^{-1}, respectively. New bands observed at 1200–1800 cm^{-1} after the reaction (Fig. 11b) indicate the formation of carbon deposits on the TiO_2 surface. Lower carbon balances in the presence of TiO_2 are ascribed to the formation of these carbon deposits. The bands at 1720 and 1420 cm^{-1} can be ascribed to some carbonyl and C–O groups, respectively, suggesting the adsorption of oxidation intermediates on TiO_2.

Comparison of Figs. 11a and b clearly shows that the surface hydroxyl groups at 3650–3700 cm^{-1} disappear during the reaction course. This kind of phenomenon has been also observed in the TiO_2-catalyzed photooxidation of benzene

in dry air [19]. We have proposed that in the photocatalytic reactions, the surface hydroxyl groups are oxidized to form OH radicals, which are responsible for the oxidative decomposition of benzene. These findings suggest that the chemical reaction occurs on the TiO_2 surface in SDR. In the photocatalytic reactions, disappearance of OH groups accompanies the formation of carbonaceous materials [19].

It has been reported that O_3 is decomposed on metal oxides such as MnO_2, Ag_2O, Fe_3O_4, TiO_2, and Cu_2O [26–28]. We have already reported that loading of MnO_2 facilitates the benzene decomposition utilizing O_3 [14]. Under the conditions where benzene decomposition was performed, 800–1800 ppm of ozone was generated from air in SDR, but no change was observed in ozone level in the absence or presence of TiO_2. This finding suggests that O_3 formed in SDR was not involved in the benzene decomposition in the present case.

Fig. 12 clearly shows the significance in hybridization of SDR with TiO_2. With SDR, the initial benzene conversion reaches 100%, but it gradually decreases and levels off at 72% after 40 min (Fig. 12a). The concentrations of CO and CO_2 concurrently increase and level off after 20 min. These findings suggest that TiO_2 can maintain its photocatalytic activity in silent discharge plasma. Fig. 12b shows the time profile for benzene decomposition with the photochemical reactor. In contrast to the SDR-TiO_2 reactor, the catalyst was almost completely deactivated in the steady state although the conversion for the first 1 min was 45%. It is impossible to directly compare the reaction rates for the benzene oxidation on TiO_2 catalyst between these systems, since the wavelength distribution and intensity of emitted light are different for each other. However, deactivation of TiO_2 in the benzene photooxidation in dry air has been generally observed [25,29]. Thus, one of the remarkable characteristics for the SDR-TiO_2 hybrid system is that the activity of TiO_2 is sustained even under dry conditions.

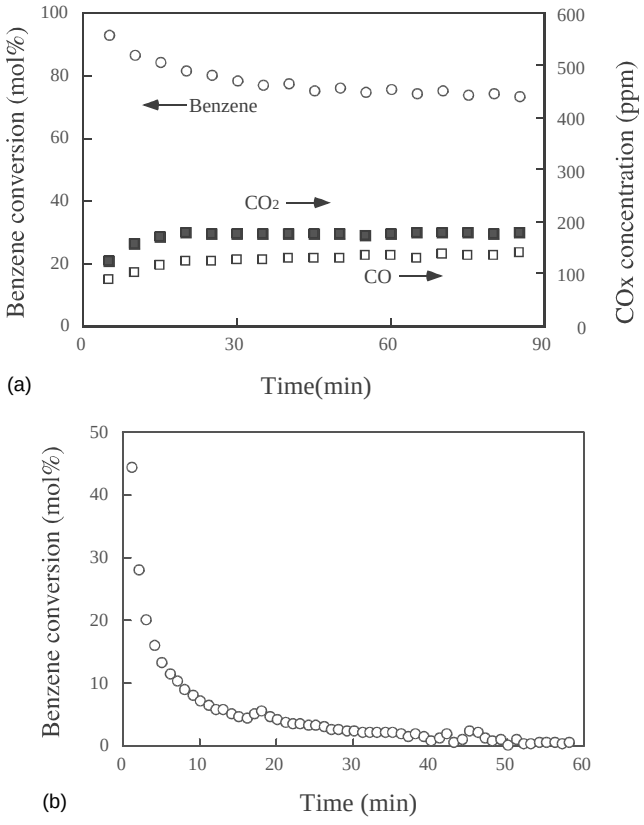

Fig. 12. Time profile for benzene decomposition in dry air. (a) Reactor SDR, gap distance: 1.0 mm, TiO_2: 70 mg (0.12 mg cm^{-2}) on the glass tube, benzene: 100 ppm, Q = 100 ml/min, RED = 0.84 kJ/l. (b) Light source 500 W high pressure Hg lamp with a 365 cutoff filter (photon flux = 0.027 Einstein min^{-1}), TiO_2: 2.0 mg cm^{-2} on the glass plate, benzene: 100 ppm, Q = 100 ml/min.

3.3. Synergy between SDR and HQA 12

HQA 12 was used to check the catalytic effect of TiO_2 pellets to be housed in punch since it was difficult to prepare for authentic TiO_2 pellets with sufficient mechanical strengths. An induction period was observed (Fig. 13), but 1.6-fold higher conversions were obtained for benzene by housing HQA 12 inside punch. Comparable data were obtained for the yields of CO and CO_2 as in the case of SDR-TiO_2 (Fig. 10b). In this style of hybridization with SDR, efficiency of light absorption is not expected to be high enough to excite TiO_2 pellets. It is necessary to increase the pinhole density on the electrode surface.

With this style of TiO_2 hybridization with SDR, no change was observed in ozone concentration levels as in the cases of no catalyst (Fig. 7). These findings suggest that the same types of active oxygen species are involved in the oxidative decomposition of benzene as in the case of TiO_2 coated on the inside wall of the SDR glass tube.

3.4. Significance in hybridization of SDR with catalysts/photocatalysts

Effects of catalyst hybridization with SDR was investigated. In nonthermal plasma, benzene shows only a medium

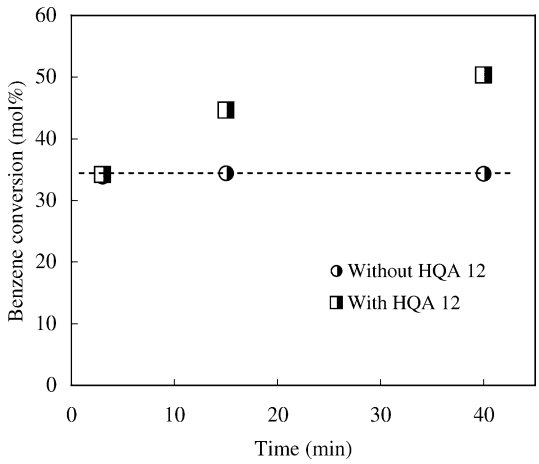

Fig. 13. Additive effect of HQA 12 on benzene conversion in air. Gap distance: 1.0 mm, benzene: 105 ppm, Q = 500 ml/min, RED = 0.32 kJ/l.

reactivity, irrespective of background gases. In this sense, it is noteworthy that the positive effects were observed in the benzene decomposition with the systems of SDR-MnO_2 and SDR-TiO_2 in the residence time range of 0.36–1.80 s. Effective utilization of active oxygen species is essential in VOCs removal, and MnO_2 and TiO_2 can generate higher concentrations of different types of active oxygen species in nonthermal plasma. It is facile and promising to simultaneously hybridize MnO_2 and TiO_2 with SDR based on the data presented in this paper. Utilization of different types of oxidation catalysts increases in situ concentrations of active oxygen species not only in the gas phase but on the catalyst surface, resulting in the higher energy efficiency and enhanced performance of SDR as an effective reactor for the oxidative decomposition of VOCs with low to medium reactivities in nonthermal plasma.

4. Conclusions

It has been shown that MnO_2, TiO_2, and TiO_2–silica gel hybridized with SDR promote benzene decomposition in air with higher selectivities of CO_2 at residence times shorter than 2 s. It is suggested that active oxygen species generated in the gaseous phase and on the catalyst surface facilitate the oxidative decomposition of benzene. Hybridization of SDR with MnO_2 or TiO_2 is effective in suppressing their deactivation.

Acknowledgements

This research was performed under the auspices of New Energy and Industrial Technology Development Organization of Japan (NEDO).

References

[1] T. Yamamoto, P.A. Lawless, M.K. Owen, D.S. Ensor, C. Boss, in: B.M. Penetrante, S.E. Schultheis (Eds.), Non-Thermal Plasma Techniques for Pollution Control, vol. 34, Part B, NATO ASI Series, Springer-Verlag, 1993, p. 139.
[2] D. Evans, L.A. Rosocha, G.K. Anderson, J.J. Coogan, M.J. Kushner, J. Appl. Phys. 74 (1993) 5378.
[3] T. Yamamoto, J.S. Chang, A.A. Berezin, H. Kohno, S. Honda, J. Adv. Oxid. Technol. 1 (1996) 67.
[4] T. Yamamoto, K. Mizuno, I. Tamori, A. Ogata, M. Nifuku, M. Michalska, G. Prieto, IEEE Trans. Ind. Appl. 32 (1996) 100.
[5] S. Futamura, T. Yamamoto, IEEE Trans. Ind. Appl. 33 (1997) 447.
[6] S. Futamura, A. Zhang, T. Yamamoto, J. Electrostat. 42 (1997) 51.
[7] S. Futamura, A. Zhang, G. Prieto, T. Yamamoto, IEEE Trans. Ind. Appl. 34 (1998) 967.
[8] S. Futamura, A. Zhang, T. Yamamoto, IEEE Trans. Ind. Appl. 36 (2000) 1507.
[9] A. Ogata, K. Yamauchi, K. Mizuno, S. Kushiyama, T. Yamamoto, IEEE Trans. Ind. Appl. 35 (1999) 1289.
[10] S.L. Suib, S.L. Brock, M. Marquez, J. Luo, H. Matsumoto, Y. Hayashi, J. Phys. Chem. B 102 (1998) 9661.
[11] S. Futamura, A. Zhang, T. Yamamoto, IEEE Trans. Ind. Appl. 35 (1999) 760.
[12] A. Zhang, S. Futamura, T. Yamamoto, J. Air Waste Manage. Assoc. 49 (1999) 174.
[13] S. Futamura, H. Einaga, A. Zhang, IEEE Trans. Ind. Appl. 37 (2001) 978.
[14] H. Einaga, T. Ibusuki, S. Futamura, IEEE Trans. Ind. Appl. 37 (2001) 1476.
[15] S. Futamura, A. Zhang, H. Einaga, H. Kabashima, Catal. Today 72 (2002) 259.
[16] S. Futamura, H. Kabashima, H. Einaga, J. Jpn. Petrol. Inst. 45 (2002) 329.
[17] J. Luo, S.L. Suib, Y. Hayashi, H. Matsumoto, J. Phys. Chem. A 103 (1999) 6151.
[18] O. d'Hennezel, P. Pichat, D.F. Ollis, J. Photochem. Photobiol. A 118 (1998) 197.
[19] H. Einaga, S. Futamura, T. Ibusuki, Phys. Chem. Chem. Phys. 1 (1999) 4903.
[20] S.L. Murov, Handbook of Photochemistry, Marcel Dekker, New York, 1973, p. 119.
[21] W.-D. Chang, S.M. Senkan, Environ. Sci. Technol. 23 (1989) 442.
[22] R. Atkinson, D.L. Baulch, R.A. Cox, R.F. Hampson Jr., J.A. Kerr, J. Troe, J. Phys. Chem. Ref. Data (1980–1992).
[23] W. Li, G.V. Gibbs, S.T. Oyama, J. Am. Chem. Soc. 120 (1998) 9041.
[24] W. Li, S.T. Oyama, J. Am. Chem. Soc. 120 (1998) 9047.
[25] H. Einaga, S. Futamura, T. Ibusuki, Chem. Lett. (2001) 582.
[26] B. Dhandapani, S.T. Oyama, Appl. Catal. B 11 (1997) 129.
[27] S. Imamura, M. Ikebata, T. Ito, T. Ogita, Ind. Eng. Chem. Res. 30 (1991) 217.
[28] B. Ohtani, S.-W. Zhang, S.-I. Nishimoto, T. Kagiya, J. Chem. Soc. Faraday Trans. 88 (1992) 1049.
[29] M.L. Sauer, D.F. Ollis, J. Catal. 163 (1996) 215.